Generation of Optical Frequency Combs in Fibres: An Optical Pulse Analysis

Marina Zajnulina[a], Michael Böhm[b], Keith Blow[c], José M. Chavez Boggio[a], Andres A. Rieznik[d], Roger Haynes[a], Martin M. Roth[a]

[a]innoFSPEC-VKS, Leibniz Institute for Astrophysics, An der Sternwarte 16, 14482 Potsdam, Germany
[b]innoFSPEC-InFaSe, University of Potsdam, Am Mühlenberg 3, 14476 Golm, Germany
[c]Aston Institute of Photonic Technologies, Aston University, Aston Triangle, Birmingham, B4 7ET, United Kingdom
[d]Instituto Tecnologico de Buenos Aires and CONICET, Buenos Aires, Argentina

ABSTRACT

The innovation of optical frequency combs (OFCs) generated in passive mode-locked lasers has provided astronomy with unprecedented accuracy for wavelength calibration in high-resolution spectroscopy in research areas such as the discovery of exoplanets or the measurement of fundamental constants. The unique properties of OCFs, namely a highly dense spectrum of uniformly spaced emission lines of nearly equal intensity over the nominal wavelength range, is not only beneficial for high-resolution spectroscopy. Also in the low- to medium-resolution domain, the OFCs hold the promise to revolutionise the calibration techniques. Here, we present a novel method for generation of OFCs. As opposed to the mode-locked laser-based approach that can be complex, costly, and difficult to stabilise, we propose an all optical fibre-based system that is simple, compact, stable, and low-cost. Our system consists of three optical fibres where the first one is a conventional single-mode fibre, the second one is an erbium-doped fibre and the third one is a highly nonlinear low-dispersion fibre. The system is pumped by two equally intense continuous-wave (CW) lasers. To be able to control the quality and the bandwidth of the OFCs, it is crucial to understand how optical solitons arise out of the initial modulated CW field in the first fibre. Here, we numerically investigate the pulse evolution in the first fibre using the technique of the solitons radiation beat analysis. Having applied this technique, we realised that formation of higher-order solitons is supported in the low-energy region, whereas, in the high-energy region, Kuznetsov-Ma solitons appear.

Keywords: Spectrograph calibration, Optical frequency combs, Soliton radiation beat analysis, Higher-order solitons, Kuznetsov-Ma solitons, Solitons in fibres, Four-wave mixing, Nonlinear Schrödinger equation

1. INTRODUCTION

OFCs generated in mode-locked lasers with relative stabilities at the level of $10^{-11}…10^{-15}$ have been demonstrated to provide high-resolution spectroscopy with wavelength calibration accuracies that correspond to radial velocity uncertainties of no more than a few cm/s[1,2,3,4,5,6,7,8]. The extremely high stability and repeatability of these devices have opened a new window of research opportunities, e.g. the measurement of the Universe's expansion history via the observation of the cosmological redshift of distant objects or the measurement of changes in the fine structure constants[9,10]. What has as yet not been widely appreciated is the fact that even low- to medium-resolution spectroscopy would gain significant benefits from the use of OFCs as calibration marks. The low- or medium-resolution OFCs can be deployed for such existing or novel instruments as PMAS, MUSE, 4MOST, a future Multiobject-Instrument for the E-ELT (ELT-MOS), etc[11,12,13].

We propose an all optical fibre-based approach for generation of OFCs that is stable, low-cost and allows to generate combs with tuneable spectral line spacing adjustable for the resolution requirements of the spectrographs in the low- and medium resolution range[14,15]. Since our approach includes only standard telecom components, it is easier to be

Advances in Optical and Mechanical Technologies for Telescopes and Instrumentation, edited by Ramón Navarro, Colin R. Cunningham, Allison A. Barto, Proc. of SPIE Vol. 9151, 91514V
 doi: 10.1117/12.2055554

implemented compared to the alternative fibre-based techniques[16,17,18,19]. A further advantage is that our system utilises less fibre material. It consists of three fibre stages: a conventional single-mode fibre, an erbium-doped fibre, and a highly nonlinear low-dispersion fibre. We use two phase-locked continuous-wave (CW) lasers with the laser frequency separation of $LFS = 80$ GHz as the light source. They deliver a deeply-modulated sine-wave as initial optical field which evolves into a train of Kuznetsov-Ma (KM) solitons as it propagates through the first stage[20]. At the same time, an OFC arises due to the four-wave mixing process (FWM)[21,22]. Via the changing of the LFS, it is possible to tune the OFC line spacing and adjust it to the resolution properties of the considered spectrograph.

To be able to control the quality and the bandwidth of the arising OFC, it is crucial to understand the formation of KM solitons out of a deeply modulated sine-wave. Usually, to study the dynamics of optical pulses in fibres, people use sech-profiles or slightly modulated sine-waves as initial condition. In the first case, single solitons evolve on a zero-background as they propagate through the fibre[23,24,25]. In the second case, the arising spatio-temporal breathers undergo periodic energy exchange with a finite background[26,27,28,29,30]. The processes that govern the solitons' dynamics are well understood in both cases. Here, we investigate spatio-temporal breathers that have no background. More precisely, we determine the soliton content of the pulse train that propagates in our system. To do so, we use the technique of the soliton radiation beat analysis (SRBA)[31].

This paper is structured as follows: in Sec. 2, we present the experimental setup for generation of OFCs in fibres and the according mathematical model, the concept of SRBA is depicted in Sec. 3 and the result are shown in Sec. 4, a conclusion is drawn in Sec. 5.

2. EXPERIMENTAL SETUP AND MATHEMATICAL MODEL

2.1 Setup

Fig. 1 presents the experimental setup for generation of broad and stable OFCs[14,15]. It consists of three coupled fibres: fibre A is a conventional single-mode fibre, fibre B is erbium-doped, fibre C is highly nonlinear and low-dispersive. The fibres are pumped by two equally intense phase-locked CW lasers. Laser 1 is fixed at the angular frequency ω_1, Laser 2 has tuneable frequency ω_2. The resulting frequency $\omega_c = (\omega_1 + \omega_2)/2$ of the initial modulated sine-wave coincides with the central wavelength at 1531 nm.

The evolution of an optical comb in the presented system obeys the following processes: the initial spectrum of two frequency lines with ω_1 and ω_2 gets broadened due to FWM as the light propagates through fibre A. The new lines are equidistantly positioned and have line spacing that coincides with the initial laser frequency separation $LFS = |\omega_2 - \omega_1|/2\pi$. The spectral broadening in the frequency domain corresponds to the pulse compression in the time domain: the initial modulated sine-wave gets reshaped to a train of KM solitons with pulse widths of a few pico-seconds and repetition rates that are equal to LFS[23,25,28]. In fibre B, the solitons get further compressed down to the femto-second range due to the increased nonlinearity which is a result of the gain experienced in fibre B. This compression yields the appearance of additional lines in the comb spectrum. In fibre C, the OFC is extremely broadened due to the FWM caused by the high nonlinearity of the fibre.

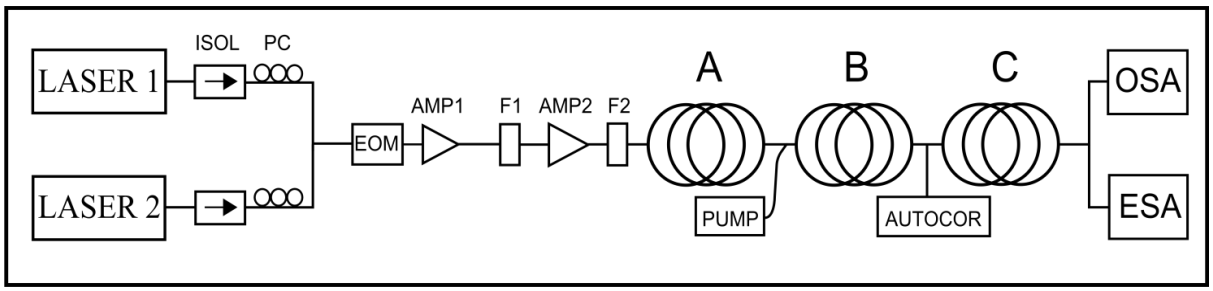

Figure 1. Experimental setup. LASER 1: fixed CW laser, LASER 2: tuneable CW laser, ISOL: optical isolator, PC: polarisation controller, EOM: electro-optical modulator, AMP1: amplifier 1, F1: optical filter 1, AMP2: amplifier 2, F2: optical filter 2, A: single-mode fibre, B: Er-doped fibre, C: highly nonlinear low-dispersion fibre, PUMP: pump laser for fibre B, AUTOCOR: optical autocorrelator, OSA: optical spectrum analyser, ESA: electrical spectrum analyser

2.2 Model

We use the generalised nonlinear Schrödinger equation (GNLS) for a slowly varying optical field envelope $A = A(z,t)$ in the co-moving frame to model the propagation of light through fibre A of the setup presented in Sec. 2.1[14,15,21,22]:

$$\frac{\partial A}{\partial z} = i\sum_{k=2}^{K}\frac{i^k}{k!}\beta_k\frac{\partial^k A}{\partial t^k} + i\gamma\left(1+\frac{i}{\omega_0}\frac{\partial}{\partial t}\right)\left(A\int_{-\infty}^{\infty}R(t')|A(t-t')|^2dt'\right), \tag{1}$$

where $\beta_k = \left(\frac{\partial^k\beta}{\partial\omega^k}\right)_{\omega=\omega_0}$ denotes the value of the dispersion order at the carrier frequency ω_0. For the dispersion order, we use $K = 10$. γ is the nonlinear coefficient defined as $\gamma = \frac{\omega_0 n_2}{c\cdot S}$ with $n_2$being the nonlinear refractive index of silica, S the effective mode area, and c the speed of light. The delayed Raman effect is incorporated into the model by means of the response function

$$R(t) = (1-f_R)\delta(t) + f_R h_R(t), \tag{2}$$

which includes both, the electronic contribution assumed to be nearly instantaneous and the contribution set by vibration of silica molecules and expressed via $h_R(t)$. $f_R = 0.245$ denotes the fraction of the delayed Raman response to the total nonlinear polarisation. The function $h_R(t)$ is defined as follows:

$$\begin{aligned} h_R(t) &= (1-f_b)h_a(t) + f_b h_b(t), \\ h_a(t) &= \frac{\tau_1^2+\tau_2^2}{\tau_1\tau_2^2}\exp\left(-\frac{t}{\tau_2}\right)\sin\left(\frac{t}{\tau_1}\right), \\ h_b(t) &= \left(\frac{2\tau_b - t}{\tau_b^2}\right)\exp\left(-\frac{t}{\tau_b}\right) \end{aligned} \tag{3}$$

with $\tau_1 = 12.2$ fs and $\tau_2 = 32$ fs being the characteristic times of the Raman response of silica and $f_b = 0.21$ representing the according vibrational instability with $\tau_b \approx 96$ fs. The initial condition for Eq. 1 is given by

$$A_0(z=0,t) = \sqrt{P_0}\sin(\omega_c t). \tag{4}$$

Eq. 4 represents the radiation of the lasers Laser 1 and Laser 2 with the equal value of peak power P_0 and the central angular frequency $\omega_c = (\omega_1+\omega_2)/2$. The numerical solution of Eq. 1 and Eq. 4 is achieved using the interaction picture method in combination with the local error method. In this paper, we choose 2^{16} sample points in a temporal window of 256 ps. To perform SRBA, we use the following parameters for fibre A: $\beta_2 = -15\,\frac{\mathrm{ps}^2}{\mathrm{km}}$, $\beta_3 = 0.1\,\frac{\mathrm{ps}^3}{\mathrm{km}}$, and $\gamma = 2\ \mathrm{W}^{-1}\mathrm{km}^{-1}$. The value of the initial laser frequency separation it set to $LFS = 80$ GHz. Eq. 1 and Eq. 4 deliver solutions of the optical field in the time domain. To extract the information about the arising OFCs, one will need to perform Fourier transform into the frequency with regards to the time variable t.

3. SOLITON RADIATION BEAT ANALYSIS

As mentioned previously, our aim is to generate stable and broadband OFCs. Generally, the spectral bandwidth of optical pulses depends on the pulse duration. In the specific case of optical solitons, the pulse duration is inversely proportional to their energy. Depending on the amount of the input power, it is possible to generate not only fundamental, but also higher-order solitons, whereby the soliton order increases with the input power. The soliton order itself is described by a real number N, the fundamental solitons have $N = 1$, whereas the higher-order ones have higher values of N. An important feature is that the energy of a solitons scales with N. In this paper, we address the question how the energy and N are related to each other.

Since the GNLS (Eq. 1) is not integrable in our case, we cannot solve it explicitly. Therefore, we take advantage of SRBA to analyse the system. SRBA is a numerical technique that can provide us with information about the energy, the velocity, the phase, and the position of each soliton involved. Since Eq. 1 is formulated in the co-moving frame, the velocity, the phase, and the position are not relevant. They can be set by the boundary conditions for each specific case.

Thus, the only important parameter left is the energy which can be related to N. The technique of SRBA can be applied for arbitrary, not only solitary, initial conditions[32].

We introduce the technique of SRBA by a simple example. Generally holds that the resolution in the frame of SRBA strongly depends on the total fibre length chosen for simulation. Precisely, it goes with $1/L$ with L being the total propagation length. Thus, to show the features of SRBA in detail, we perform a calculation with a fibre length of $L = 100$ km, which will allow us to produce well resolved graphs. The input power is set to $P_0 = 1.5$ W, all other fibre parameters are chosen as stated in Sec. 2.

To perform the SRBA, we start with the calculation of the optical field propagating through the fibre, i.e. $A(z,t)$. After calculating the power values $P(z,t) = |A(z,t)|^2$, we extract $P(z) = P(z,t=0)$. These values are presented in Fig. 2 as a dashed line. As one can see, the power function $P(z)$ oscillates over the propagation distance. This oscillation contains information about the involved solitons and their properties. To decode this imprinted information, we perform a Fourier transform on these data. The power spectrum of the Fourier transform over the spacial frequencies Z, $\hat{P}(Z)$, is shown in Fig. 3 again as a dashed line.

Let us now consider the low-frequency region. Obviously, the strong oscillation of $P(z)$ over the propagation distance (see Fig. 2) results in a peak in the spacial frequency domain (see Fig. 3). Additionally to the peaks, there is a background which is an artifact of the Fourier transform. It arises due to the discontinuity of $P(z)$ at the boundaries. To suppress this artificial background, we apodise $P(z)$ by means of a Gaussian apodisation function that is presented as a solid line in Fig. 2. As one can see, the discontinuity of the apodised power $P_{apo}(z)$ is effectively minimised at the boundaries. Now, the apodised power $P_{apo}(z)$ gets Fourier-transformed exactly as the not-apodised one. The according power spectrum is also shown in Fig. 3 as a solid line. The background of the transformed apodised data is drastically reduced and more peaks are visible now. However, to get an unambiguous mapping of solitons and their beating frequencies, it is necessary to perform the described algorithm for different values of the input power P_0. This will be presented in Sec. 4.

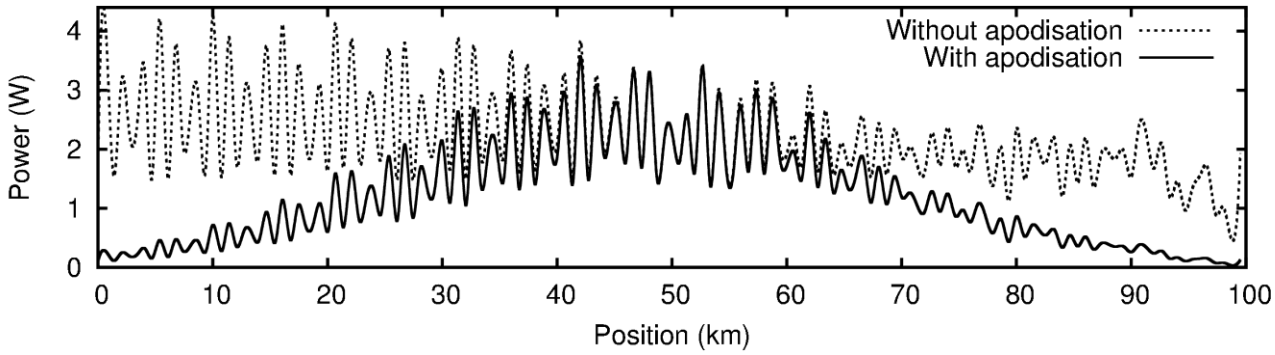

Figure 2. Pulse peak power at $t = 0$ over propagation distance. Dashed line: non-apodised peak power, solid line: apodised power

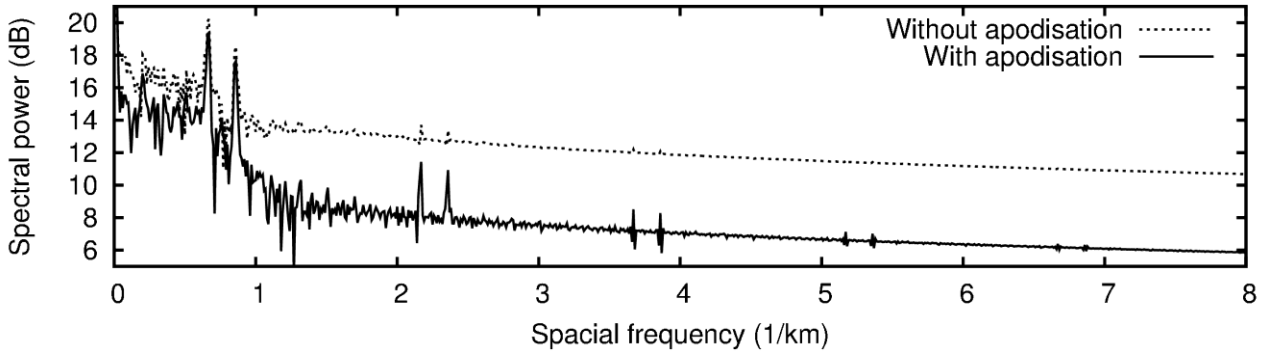

Figure 3. The power spectrum obtained by the Fourier transform of the functions presented in Fig. 2. Dashed line: non-apodised peak power, solid line: apodised power

4. RESULTS

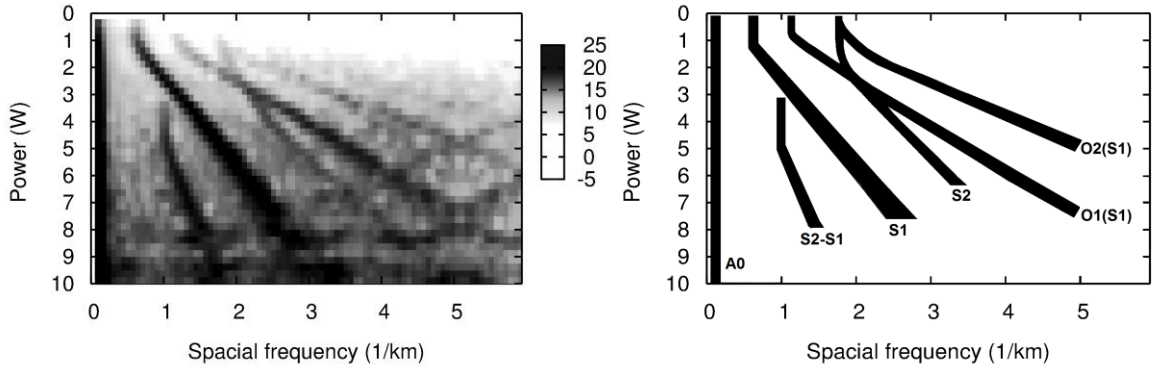

Figure 4. Left: Power spectrum of the Fourier transform in grayscale for different values of input power P_0, Right: Sketch of main peaks. A0: Average power, S1: soliton 1, S2: solitons 2, O1(S1): first overtone of S1, O2(S1): second overtone of S1, S2-S1: mixing frequency of S1 and S2

Now using the SRBA technique presented in Sec. 3, we analyse our system for input power values of $0.25\,\mathrm{W} \leq P_0 \leq 10\,\mathrm{W}$, whereas the total fibre length is chosen to be $L = 15\,\mathrm{km}$. SRBA will answer the general question if optical solitons can be generated in our system. In the case that solitons are present, SRBA will provide us with information about the energy content of the invloved solitons and the according soliton order.

The results of the extended numerical simulations are summerised in Fig. 4 (left). The power spectrum of the Fourier transform as a function of spacial frequency Z and the input power P_0 is shown as a density plot in grayscale. For any values of P_0 and $Z = 0$, a strong peak (A0) is visible that corresponds to the average value of the power $P(Z)$. Since it does not contain any pieces of information about the soliton content, we exclude it from our consideration. In contrast, all other peaks give us a clue about the involved solitons and the dispersive radiation. To illustrate the mapping of the peaks, we use a simplified version presented in Fig. 4 (right).

The most prominent peak starting at $P_0 = 0.25\,\mathrm{W}$ and $Z = 0.6\,\mathrm{km}^{-1}$ corrsponds to the beating of soliton S1 and the background. In the input power region $0.25\,\mathrm{W} \leq P_0 < 1.3\,\mathrm{W}$, the spacial frequecy Z of S1 does not depend on the input power, for any other values of P_0, Z scales nearly linearly with P_0. Obviously, at $P_0 = 1.3\,\mathrm{W}$, a transition between two different soliton states takes place.

In case of a single soliton propagating through the fibre, such transition would not be expected. Instead, a positiv threshold value of the input power, $P_0 > 0\,\mathrm{W}$, should be present from which the soliton formation is supported[31,33]. In our case, however, we consider a train of pulses that acts as a collective soliton state. In such a collective state, single parts of the pulses overlap to the structures which have in total enough energy to form a soltion. Apparently, this is the reason why a transion between two soliton states and not a threshold occurs.

The overtones of S1 arise at $P_0 = 0.25\,\mathrm{W}$ and $Z = 1.2\,\mathrm{km}^{-1}$ (O1) and $P_0 = 0.25\,\mathrm{W}$ and $Z = 1.8\,\mathrm{km}^{-1}$ (O2). The appearance of the overtones is a feature of SRBA and gives us no further information about the soliton content. The second soliton (S2) arises exactly at the point where O2 appears, i.e. at $P_0 = 0.25\,\mathrm{W}$ and $Z = 1.8\,\mathrm{km}^{-1}$. The spacial frequency difference between the first and second soltion, i.e. S1 and S2, leads to a mixing frequency that is visible from $P_0 = 3.5\,\mathrm{W}$ and $Z = 1.0\,\mathrm{km}^{-1}$ (S2-S1). Like the soliton overtones, mixing frequencies are an artifact of SRBA.

It is known that the spacial frequency Z is proportional to the energy of a soltion[31,33]. In our case, at $P_0 = 0.25\,\mathrm{W}$, the ratio R between the spacial frequencies of S1 and S2 is $R = 1:3$. Such ratio typically appears for higher-order solitons with $N = 2$. Therefore, we conclude that, in our case, S1 and S2 constitute a soliton with $N = 2$. R is constant for in the input power region of $0.25\,\mathrm{W} \leq P_0 < 1.3\,\mathrm{W}$. For higher values of P_0, the ratio R decreases to $R < 1:2$. Obviously, there is change in the soliton composition for any input powers $P_0 > 1.3\,\mathrm{W}$. As for KM solitons specifically, there is one

degree of freedom that determines the behaviour of the solutions of Eq. 1[28]. As just mentioned, we observe solitons with changing poperties expressed via the ratio R for different values of the input power $P_0 > 1.3$ W. These changes are consistent with the mentioned degree of freedom of KM solitons. Therefore, we conclude that, in our case, the formation of exactly KM solitons and not of any other soliton types is supported for higher values of the input power.

5. CONCLUSION

We numerically studied the formation of optical solitons in a system that can be deployed for generation of optical frequency combs useful for astronomical application in the low- and medium resolution range. These studies were performed using the soliton radiation beat analysis. We were able to show that for any chosen values of the input power, the soliton formation is supported. This is a positive feature of our system, because solitons generally provide stable and broad spectra. We identified two soliton regimes and a transition point between them. For input power values $P_0 < 1.3$ W (low-energy region), the formation of higher-order solitons with the order $N = 2$ occurs, whereas the formation of Kuznetsov-Ma solitons is supported for any input power values of $P_0 > 1.3$ W (high-energy region). The regime transition point lies, accordingly, at $P_0 = 1.3$ W. Since the optical frequency bandwidths go with the increasing input power, it is preferable to choose the region in which the generation of the Kuznetsov-Ma solitons occurs for the purpose of astronomical applications. Moreover, from the stability point of view, it is advisable to deploy standard telecom fibres for generation of optical frequency combs, since for such fibres, we observed no soliton fission in our simulations that might degrade the system behaviour.

ACKNOWLEDGEMENTS

We acknowledge the financial support of the German Federal Ministry of Education and Research (Grant 03ZAN11).

REFERENCES

[1] Holzwarth, R., Udem, T., and Hänsch, T. W., "Optical frequency synthesizer for precision spectroscopy", Physical Review Letters, Vol. 85, No. 11(2000)

[2] Cundiff, S. T. and Yen, J., "Colloquium: femtosecond optical frequency combs", Reviews of Modern Physics, Vol. 75 (2003)

[3] Osterman, S., Diddams, S., Beasley, M., Froning, C., Hollberg, L., MacQueen, P., Mbele, V., and Weiner, A., "A proposed laser frequency comb based wavelength reference for high resolution spectroscopy", Proc. of SPIE 6693, 66931G-1 (2007)

[4] Murphy, M. T., Udem, T., Holzwarth, R., Sizmann, A., Pasquini, L., Araujo-Hauck, C., Dekker, H., D'Odorico, S., Fischer, M., Hänsch, T. W., and Manescau, A., "High-precision wavelength calibration of astronomical spectrographs with laser frequency combs", Monthly Notices of the Royal Astronomical Society, Vol. 380, No. 2 (2007)

[5] Braje, D. A., Kirchner, M. S., Osterman, S., Fortier, and T., Diddams, A., "Astronomical spectrograph calibration with broad-spectrum frequency combs", European Physical Journal D, Vol. 48, Issue 1 (2008)

[6] Wilken, T., Lovis, C., Manescau, A., Steinmetz, T., Pasquini, L., and Lo Curto, G., "High-precision calibration of spectrographs using laser frequency combs", Proc. Of SPIE, Vol. 7735, 77350T-1 (2010)

[7] Doerr, H.-P., Kentischer, T. J., Steinmetz, T., Probst, R. A., Franz, M., Holzwarth, R., Udem, T., Hänsch, T. W., and Schmidt, W., "Performance of a laser frequency comb calibration system with a high-resolution solar echelle spectrograph", Proc. of SPIE, Vol. 8450, 84501G (2012)

[8] Lo Curto, G., Manescau, A., Avila, G., Pasquini, L., Wilken, T., Steinmetz, T., Holzwarth, R., Probst, R., Udem, T., Hänsch, T. W., González Hernández, J. I., Esposito, M., Rebolo, R., Canto Martins, B., de Medeiros, J. R., "Achieving a few cm/sec calibration repeatability for high resolution spectrographs: the laser frequency comb on HARPS", Proc. of SPIE 8446, 84461W (2012)

[9] Steinmetz, T., WIlken T., Araujo-Hauck, A., Holzwarth, R., Hänsch, T. W., Pasquini, L., Manescau, A., D'Odorico, S., Murphy, M. T., Kentischer, T., Schmidt, W., and Udem, T., "Laser frequency combs for astronomical observations", Science, Vol. 321, No. 5894 (2008)

[10] Griest, K., Whitmore, J. B., Wolfe, A. M., Prochaska, J. X., Howk, J. C., and Marcy, G. W., "Wavelength accuracy of the Keck HIRES spectrograph and measuring changes in the fine structure constant", The Astrophysical Journal, 708:158–170 (2010)
[11] Roth, M. M., Kelz, A., Fechner, T., Hahn, T., Bauer, S.-M., Becker, T., Böhm, P., Christensen, L., Dionies, F., Paschke, J., Popow, E., Wolter, D., Schmoll, J., Laux, U., Altmann, W., „PMAS: The Potsdam Multi-Aperture Spectrophotometer. I. Design, Manufacture, and Performance", Publications of the Astronomical Society of the Pacific, Vol. 117, Issue 832 (2005)
[12] Kelz, A., Bauer, S. M., Biswas, I., Fechner, T., Hahn, T., Olaya, J.-C., Popow, E., Roth, M. M., Streicher, O., Weilbacher, P., Bacon, R., Laurent, F., Laux, U., Lizon, J. L., Loupias, M., Reiss, R., Rupprecht, G., „The calibration unit and detector system tests for MUSE", Proc. of SPIE 7735, 773552 (2010)
[13] de Jong, R. S., Bellido-Tirado, O., Chiappini, C., Depagne, E, Haynes, R., et al., "4MOST – 4-meter Multi-Object Spectroscopic Telescope", Proc. of SPIE 8446, 84460T (2012)
[14] Zajnulina, M., Chavez Boggio, J. M., Rieznik, A. A., Haynes, R. and Roth, M. M., "Generation of optical frequency combs in fibres", Proc. of SPIE 8775, 87750C (2013)
[15] Chavez Boggio, J. M., Rieznik, A. A., Zajnulina, M., Böhm, M., Bodenmüller, D., Wysmolek, M., Sayinc, H., Neumann, J., Kracht, D., Haynes, R. and Roth, M. M., "Generation of an astronomical optical frequency comb in three fibre-based nonlinear stages", Proc. of SPIE 8434, 84340Y (2012)
[16] Finot, C., Fatome, J., Pitois, S., and Millot, G., "All-Fibered High-Quality Low Duty-Cycle 20-GHz and 40-GHz Picosecond Pulse Sources", IEEE Photonics Technology Letters, Vol. 19, No. 21 (2007)
[17] Fortier, C., Kibler, B., Fatome, J., Finot, C., Pitois, S., and Millot, G., "All-fibered high-quality duty-cycle 160-GHz femtosecond pulse source", Laser Phys. Lett. 5, No. 11 (2008)
[18] Mansouri, El I., Fatome, J., Finot, C., Lintz, M., and Pitois, S., "All-Fibered High-Quality Stable 20- and 40-GHz Picosecond Pulse Generators for 160-Gb/s OTDM Applications", IEEE Photonics Technology Letters, Vol. 23, No. 20 (2011)
[19] Fatome, J., Pitois, S., Fortier, C., Kibler, B., Finot, C., Millot, G., Courde, C., Lintz, M., and Samain, E., "Multiple four-wave mixing in optical fibers: 1.5-3.4-THz femtosecond pulse sources and real-time monitoring of 20-GHz picosecond source", Optics Communications 283 (2010)
[20] Kibbler, B., Fatome, J., Finot, C., Millot, G., Genty, G., Wetzel, B., Akhmediev, N., Dias, F., and Dudley, "Observation of Kuznetsov-Ma solitons dynamics in optical fibre", Scientific Reports 2, No. 463 (2012)
[21] Agrawal, G. P., [Nonlinear Fiber Optics], Academic Press (2013)
[22] Agrawal, G. P., [Applications of Nonlinear Fiber Optics], Academic Press (2008)
[23] Mollenauer, L. F., Stolen, R. H., Gordon, J. P. and Tomlinson, W. J., „Extreme picosecond pulse narrowing by means of soliton effect in single-mode optical fibers", Optics Letters, Vol. 8, No. 5 (1983)
[24] Blow, K. J. and Wood, D., " The evolution of solitons from non-transform limited pulses", Optics Communications, Vol. 58, No. 5 (1986)
[25] Voronin, A. A. and Zheltikov, A. M., "Soliton-number analysis of soliton-effect pulse compression to single-cycle pulse width", Physical Review A 78, 063834 (2008)
[26] Akhmediev, N. and Korneev, V. I., "Modulation instability and periodic solutions of the nonlinear Schrödinger equation", Theor. Math. Phys., Vol. 69, No. 2 (1986)
[27] Dudley, J. M., Genty, G., Dias, F., Kibler, B., Akhmediev, N., "Modulation instability, Akhmediev breathers and continuous wave supercontinuum generation", Optics Express, Vol. 17, No. 24 (2009)
[28] Kibler, B., Fatome, J., Finot, C., Millot, G., Dias, F., Genty, G., Akhmediev, N., and Dudley, J. M., "The Peregrine solitons in nonlinear fibre optics", Nature Physics, Vol. 6 (2010)
[29] Hammani, K., Kibler, B., Finot, C., Morin, P., Fatome, J., Dudley, J. M., and Millot, G., "Peregrine solitons generation and breakup in standard telecommunications fiber", Optics Letters, Vol. 36, Issue 2 (2011)
[30] Mahnke, C. and Mitschke, F., "Possibility of an Akhmediev breather decaying into solitons", Physical Review A 85, 033808 (2012)
[31] Böhm, M. and Mitschke, F., "Soliton-radiation beat analysis", Phys. Rev. E 73, 066615 (2006)
[32] Böhm, M. and Mitschke, F., "Soliton content of arbitrarily shaped light pulses in fibers analysed using a soliton-radiation beat pattern ", Appl. Phys. B 86, (2007)
[33] Taylor, J. R., [Optical Solitons – Theory and Experiment], Cambridge University Press (1992)